tvst

Special Issue

Selective Large-Area Retinal Pigment Epithelial Removal by Microsecond Laser in Preparation for Cell Therapy

Christian Burri[1,2,*], Sami Al-Nawaiseh[3,4,*], Philip Wakili[3], Simon Salzmann[1], Christina Krötz[5], Boris Považay[1], Christoph Meier[1], Martin Frenz[2], Peter Szurman[3,6], André Schulz[3,6], and Boris Stanzel[3,6]

[1] Institute for Human Centered Engineering (HuCE)–optoLab, Bern University of Applied Sciences, Biel, Switzerland
[2] Biomedical Photonics Group, Institute of Applied Physics, University of Bern, Bern, Switzerland
[3] Eye Clinic Sulzbach, Knappschaft Hospital Saar, Sulzbach, Saar, Germany
[4] Department of Ophthalmology, University of Münster, Münster, Germany
[5] Fraunhofer Institute for Biomedical Engineering, Sulzbach, Saar, Germany
[6] Klaus Heimann Eye Research Institute, Sulzbach, Saar, Germany

Correspondence: Boris Stanzel, Eye Clinic Sulzbach, Knappschaft Hospital Saar, An der Klinik 10, Sulzbach 66280, Germany.
e-mail: boris.stanzel@kksaar.de

Received: June 9, 2021
Accepted: October 16, 2021
Published: November 29, 2021

Keywords: cell therapy; RPE removal; RPE transplantation; selective retina therapy; laser microsurgery

Citation: Burri C, Al-Nawaiseh S, Wakili P, Salzmann S, Krötz C, Považay B, Meier C, Frenz M, Szurman P, Schulz A, Stanzel B. Selective large-area retinal pigment epithelial removal by microsecond laser in preparation for cell therapy. Transl Vis Sci Technol. 2021;10(10):17, https://doi.org/10.1167/tvst.10.10.17

Purpose: Cell therapy is a promising treatment for retinal pigment epithelium (RPE)-associated eye diseases such as age-related macular degeneration. Herein, selective microsecond laser irradiation targeting RPE cells was used for minimally invasive, large-area RPE removal in preparation for delivery of retinal cell therapeutics.

Methods: Ten rabbit eyes were exposed to laser pulses 8, 12, 16, and 20 µs in duration (wavelength, 532 nm; top-hat beam profile, 223 × 223 µm^2). Post-irradiation retinal changes were assessed with fluorescein angiography (FA), indocyanine green angiography (ICGA), and optical coherence tomography (OCT). RPE viability was evaluated with an angiographic probit model. Following vitrectomy, a subretinal injection of balanced salt solution was performed over a lasered (maximum 13.6 mm^2) and untreated control area. Bleb retinal detachment (bRD) morphology was then evaluated by intraoperative OCT.

Results: Within 1 hour after irradiation, laser lesions showed FA and ICGA leakage. OCT revealed that large-area laser damage was limited to the RPE. The angiographic median effective dose irradiation thresholds (ED_{50}) were 45 µJ (90 mJ/cm^2) at 8 µs, 52 µJ (104 mJ/cm^2) at 12 µs, 59 µJ (118 mJ/cm^2) at 16 µs, and 71 µJ (142 mJ/cm^2) at 20 µs. Subretinal injection over the lasered area resulted in a controlled, shallow bRD rise, whereas control blebs were convex in shape, with less predictable spread.

Conclusions: Large-area, laser-based removal of host RPE without visible photoreceptor damage is possible and facilitates surgical retinal detachment.

Translational Relevance: Selective microsecond laser-based, large-area RPE removal prior to retinal cell therapy may reduce iatrogenic trauma.

Introduction

In recent years, regenerative medicine has become a very promising and advanced scientific research topic. This is also the case for retinal degenerative diseases such as age-related macular degeneration (AMD).[1–5] Especially for the treatment of advanced atrophic AMD, a possible therapeutic approach lies in stem cell–derived retinal pigment epithelium (SC-RPE) cells.[5] On one hand, the RPE cell layer, which is embedded in the retina, is considered to be the origin of many retinal diseases. On the other hand, however, compared with the highly complex neuronal retina, it represents a rather convenient target for cell replacement therapy. Beside the RPE monolayer sheet transplantation approach,[6–8] SC-RPE can be injected as a suspension. This is currently being

investigated in several academic centers around the world.[9,10]

Although there are already promising results regarding RPE stem cell therapy in AMD, a methodology with minimum impact on surrounding tissues for the desirable removal of the diseased host RPE cells preceding the recolonization is still missing. Attempts for selective RPE excision have been made with various surgical tools, such as hydraulic debridement,[11,12] or chemically with sodium iodate[13,14] and ethylenediaminetetraacetic acid.[15] However, these methods are unsatisfactory due to handling complications and unintentional side effects, such as proliferative vitreoretinopathy or retinal toxicity.[11,13]

Therefore, as a novel approach for the preparation of retinal cell therapy with RPE cell suspensions, we attempted to selectively remove the RPE over a large area with single microsecond laser pulses to reduce choroidal retinal adhesion without causing detectable alterations of the choriocapillaris or the neuroretina.

Laser applications in the eye have been pursued for decades due to their elegance of direct access through the ocular media and the ability of micrometer-precise positioning under optical control. Depending on the laser parameters applied, the resulting tissue effect and therefore the clinical outcome can vary greatly. To best meet the requirements for RPE-specific breakdown, the approach known as selective retina therapy (SRT) is particularly suitable. SRT intends to selectively affect the 10-µm-thick RPE monolayer while sparing the neuroretina and especially the photoreceptors, as well as choroid.[16,17] This laser method was developed at the Medical Laser Center Lübeck (Lübeck, Germany) and was successfully tested in vivo for the first time by Roider et al.[18] in 1992. The aim of the method is to rejuvenate the regenerative RPE, resulting in improved metabolism at the target sites after RPE migration and proliferation.[17,19] The basis for this selective RPE damage is provided by the intracellular melanosomes, which absorb about 50% of the incident light in the green spectral range.[20] Within the thermal confinement of SRT, peak temperatures (≈150°C) at the melanosomes in the RPE initiate microsecond-long microbubble formation (MBF).[21,22] The rapid mechanical expansion and collapse of these micrometer-sized microbubbles then causes RPE cell-wall disruption, followed by immediate or delayed cell death.[22] SRT, however, typically treats only subpopulations of RPE cells and does not focus on altering the mechanical behavior, especially the adhesion strength between a large continuous region of retina and choroid.

In this work, we describe the use of large-area RPE removal utilizing microsecond laser pulses, similar to SRT in terms of selectivity but not regarding the rejuvenation approach, as the goal is reduced choroidal retinal adhesion for RPE cell suspension. Thus, we relied on the current trend in the field of SRT, which evaluates new compact pulsed laser sources with high continuous wave (CW) power (up to 30 W) and variable pulse duration in the microsecond range (2 to 50 µs).[23,24] For large-area treatment, a closed multispot pattern without spacing between individual lesions was applied in a controlled manner. A similar approach for large-area (2 × 2 mm) RPE and photoreceptor damage has already been investigated by the Palanker group by using a scanning laser, with the objective to create an animal model with local retinal degeneration.[25]

Following laser treatment, a subretinal injection was made within the laser-treated RPE layer, and the extension of the bleb retinal detachment (bRD) formation was then analyzed and compared with injections performed without prior laser delamination.

Materials and Methods

Animals

In this study, chinchilla bastard hybrid rabbits were used. The rabbit eye is a frequently used model in RPE transplantation studies. It is only slightly smaller than a human adult eye and offers sufficient space within the vitreous cavity for pars plana vitrectomy and induction of subretinal blebs.[26] The density and location of light-absorbing pigments in the fundus are rather uniform and comparable to those of the human eye.[20] Furthermore, they are known to form a visual streak (VS), approximately 3 mm inferior to the optic nerve head (ONH), where the rod and cone photoreceptor, ganglion cell, and amacrine cell density is highest.[27–31]

We used animals (12–16 months old, 2.0–2.5 kg; Charles River Germany GmbH, Sulzfeld, Germany) that had similar levels of retinal maturation. All procedures were approved by the state regulatory authorities of Tübingen, Germany, under study code AK 14/18 G and were in accordance with the ARVO Statement for the Use of Animals in Ophthalmic and Vision Research. The animals were anesthetized with ketamine (25 mg/kg) and xylazine (2 mg/kg). The animals were placed onto a special holding system (HuCE–optoLab, Bern University of Applied Sciences, Biel, Switzerland) that allowed stable positioning in front of the treatment system. During the treatment, the cornea was hydrated every 5 minutes with Opticel (OphthalmoPro GmbH, St. Ingbert, Germany). The eyes of the animals were kept open and fixed using a speculum. In eight out of nine rabbits, only the left eyes were treated, and the right eyes served as

untreated controls. In one rabbit, both eyes were treated because of an early euthanasia due to abnormal tooth growth.

Laser Treatment

The laser treatment system used in this study was a non-commercial prototype laser treatment system, SPECTRALIS CENTAURUS (HuCE–optoLab).[32] It consists of the upgraded diagnostic imaging platform (SPECTRALIS HRA+OCT; Heidelberg Engineering, Heidelberg, Germany) which has been extended with an experimental SRT laser (modified Merilas 532 shortpulse ophthalmic laser photocoagulator; Meridian Medical, Thun, Switzerland). The SRT laser emits light at a 532-nm wavelength, with 30 W of peak power and selectable modes for CW or SRT operation. In SRT mode, the laser supports pulses 2 to 20 µs in duration. However, due to the limited power of the treatment laser, the minimal pulse duration for the experiments presented here was set to 8 µs. At this pulse duration, radiation exposures are possible that appear clinically useful and should allow application to the human retina. Evidence for this can be found in a recently published review chart by Seifert et al.[23] for pulsed laser sources with high CW power and variable pulse duration with extrapolated clinical radiation exposure ranges based on in vivo SRT patient data. In terms of spot size, the system achieved a square top-hat beam profile of 223 × 223 µm^2 on the rabbit retina. This spot size dimension was verified by averaging the indocyanine green angiography (ICGA) measurements of all applied laser parameters. The treatment laser, after passing the imaging optics of the system, achieves an intensity modulation factor of 1.3, which indicates an almost homogeneous top-hat beam profile.[33,34] A specially developed treatment software (HuCE–optoLab) allowed planning of different treatment patterns by using the integrated infrared reflectance (IR) confocal scanning laser ophthalmoscope (cSLO).

The animals were treated in two steps. First, an RPE damage threshold pattern was applied to the rabbit retina to determine the target energy for the large-area RPE removal, which was then performed in a second step.

As depicted in the color fundus photography (CFP) in Figure 1a, the threshold pattern was located inferior to the ONH rim in the VS area. The pattern included a probe region and marker lesions (Fig. 1b). Within the probe region, single laser pulses with increasing durations from left to right (8, 12, 16, and 20 µs) and increasing pulse energy, respectively, radiant exposure from top (10 µJ ≙ 20 mJ/cm^2) to bottom (maximum 127 µJ ≙ 255 mJ/cm^2 at 20 µs) were applied. The maximum pulse energy for the threshold pattern was previously determined utilizing the same rabbit model. Prior to laser application, the pulse energy was measured with a calibrated energy meter (J-10MB-LE; Coherent, Santa Clara, CA) in front of the laser aperture of the system. The energy meter has a measurement accuracy of 2.8% at 532 nm. The radiant exposure values per lesion are detailed in Supplementary Table S1.

During the application of the threshold pattern, the live IR cSLO image was examined for changes in the backscattered IR light. The appearance of the light reflectivity in the cSLO fundus image triggers cellular RPE damage because of the occurrence of MBF, which leads to transient reflectance modulations.[21,35,36] This information was used to determine the target energy for large-area RPE removal. Figures 1c to 1e show an example of how hyporeflectivity in the IR cSLO live image changed over a short period of time. In this case, for example, RPE damage could be identified for pulse energies larger than 55 µJ (111 mJ/cm^2) for pulses of 8 µs duration (Fig. 1d, lesion 9). Based on this information, the target energy for large-scale RPE removal was determined individually for each animal. Figure 1a shows a CFP of a rabbit fundus with the application site of the threshold pattern and the region for large-area RPE removal. The large-area RPE removal was always performed temporal to the threshold pattern to facilitate surgical handling. Rectangular to square multispot patterns were applied with sizes ranging from 8.1 mm^2 (see Fig. 4) to 13.6 mm^2 (corresponding to a maximum of 266 laser lesions) (Fig. 2) without spacing between individual lesions. The lesions contained in each pattern were applied in a pulse-by-pulse fashion with a pulse duration of 8 µs. This pulse duration was chosen because RPE cell damage is more strongly associated with MBF at shorter pulse durations, and thermal tissue damage increases again at longer pulse durations.[23,36] Longer pulse durations (up to 20 µs) that were additionally applied in the threshold pattern served the investigation of this circumstance and will be addressed later in discussion section.

Evaluation of Large-Area RPE Cell Removal

IR, optical coherence tomography (OCT), FA, and ICGA images were acquired within 1 hour after laser exposure with a combined spectral domain OCT (SD-OCT) and cSLO imaging system (SPECTRALIS OCT2 module; Heidelberg Engineering). The system is able to acquire FA (486 nm), ICGA (786 nm), and IR (815 nm) images, as well as cross-sectional SD-OCT

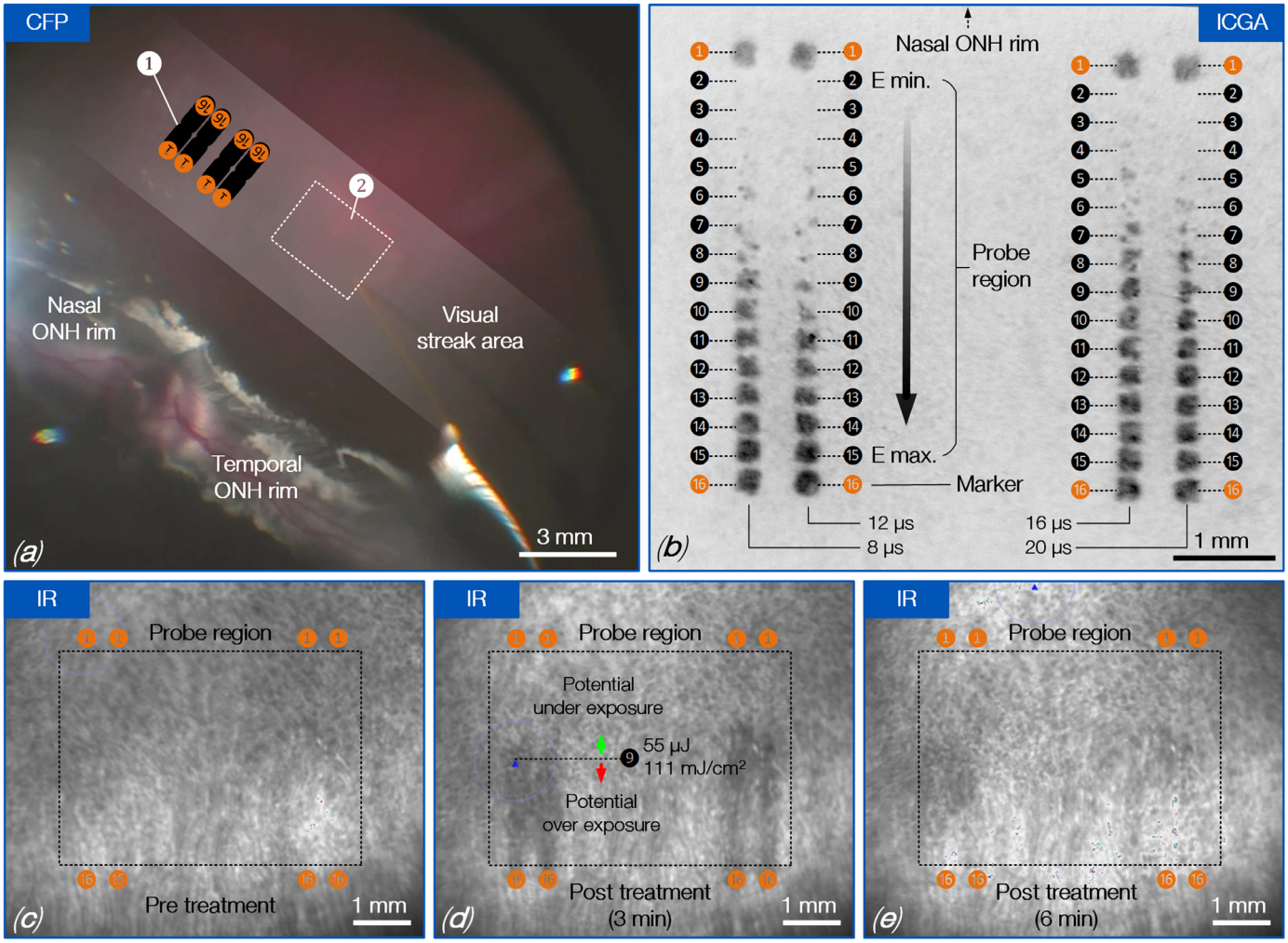

Figure 1. Threshold pattern applied to determine the target energy for large-area RPE removal. (a) CFP of a rabbit fundus. The threshold pattern (*label 1*) and the region for large-area RPE removal (*label 2*) are located inferior to the ONH rim on the VS. (b) The threshold pattern included a probe region and external marker lesions, which were applied via single laser pulses of 8, 12, 16, and 20 µs. Within the probe region, the treatment energy was increased from top (minimum 10 µJ ≙ 20 mJ/cm^2) to bottom (maximum 127 µJ ≙ 255 mJ/cm^2) at 20 µs. IR cSLO (λ = 815 nm) images: (c) before treatment, (d) 3 minutes after treatment, and (e) 6 minutes after treatment. In (d), the *dotted line* (indicating lesion 9 at 8 µs) shows the threshold for MBF. The *green* and *red lines* show the direction to potential under- and overexposure.

images. An 880-nm super luminescent diode is used for SD-OCT imaging with a fast scanning speed of 85,000 Hz, providing highly detailed images (axial resolution, 3.9 µm/pixel; lateral resolution, 5.7 µm/pixel) of the retinal structure. Angiographic images were obtained immediately following an injection of 0.2 mL sodium fluorescein solution (10%) (Alcon Pharma GmbH, Freiburg, Germany) and 0.5 mL balanced salt solution (BSS) containing 1.25 mg of indocyanine green (Diagnostic Green GmbH, Aschheim-Dornach, Germany) into the marginal ear vein. Multimodal images were acquired at every minute for a period of at least 30 minutes by using the SPECTRALIS standard objective lens, providing a 30° field of view.

Surgery

Following imaging, the rabbits underwent surgery under continued general anesthesia with ketamine (25 mg/kg) and xylazine (2 mg/kg), as noted before. Triamcinolone-assisted, 25-gauge three-port vitrectomy (Megatron 4; Geuder AG, Heidelberg, Germany) was performed in the left eye, including induction of a posterior vitreous detachment, as previously described.[37] Subsequently, localized bleb-shaped retinal detachments were created by manual subretinal injection of 15 to 30 µL ophthalmic-grade BSS (Alcon Deutschland GmbH, Freiburg im Breisgau, Germany) via a 25/38-gauge subretinal cannula (MedOne Surgical, Sarasota, FL) connected to a 100-µL syringe

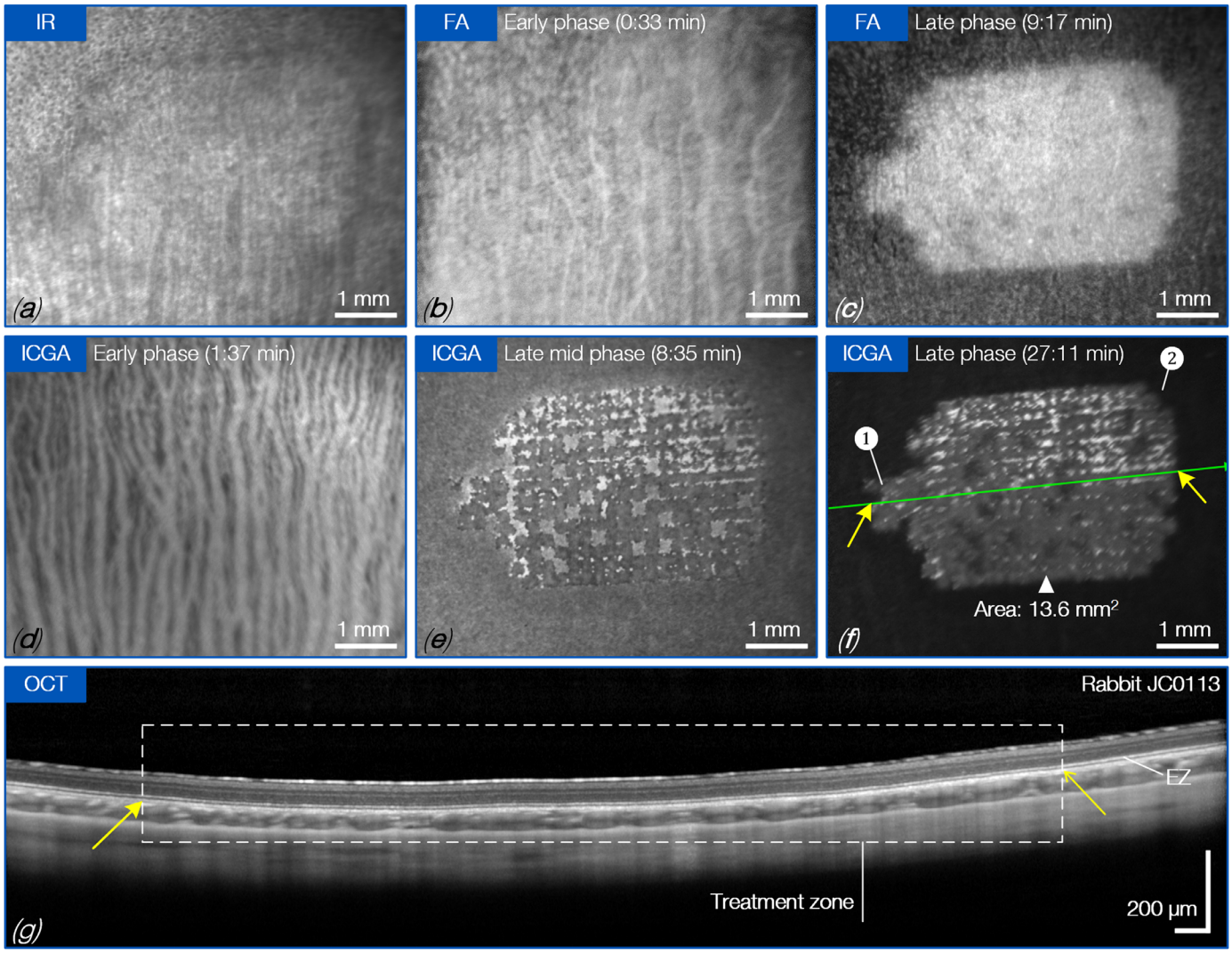

Figure 2. Multimodal imaging of large-area RPE removal after laser exposure. (a) IR showed mild hyporeflectivity, mostly at the pattern border. (b) Early phase FA showed normal choroidal filling. (c) Late phase FA showed hyperreflectivity over the treated area. (d) Early phase ICGA showed no choroidal damage or non-perfusion after laser treatment. (e) For late phase and mid phase ICGA, the treatment pattern began to occur. (f) For late phase ICGA, the treatment pattern was clearly visible. *Label 1* indicates the bottle neck, which served as a landing area for the subretinal cannula. The laser-irradiated area was 13.6 mm^2 (*label 2*). Single laser pulses of 8 µs duration with a pulse energy of 61 µJ (123 mJ/cm^2) were applied. (g) The *green line* demarcates the displayed cross-section in the corresponding SD-OCT B-scan image. The *yellow arrows* point to the border of the treated zone. The B-scan through the treatment zone shows no visible morphological changes of the retina beyond the ellipsoid zone (EZ).

(Hamilton Germany GmbH, Gräfelfing, Germany) over the large-area lasered and un-lasered control areas by a single surgeon (BVS). The injection was performed manually by the surgeon holding the syringe in the non-dominant hand and the subretinal cannula in the dominant hand; the eye was illuminated with a chandelier endoillumination probe. The bRD formation and three-dimensional morphology were evaluated by an integrated surgical microscope and intraoperative SD-OCT (OPMI-Lumera RESCAN 700 with integrated intraoperative OCT; Carl Zeiss Meditec, Jena, Germany) through a non-contact, wide-angle 128° fundus lens (RESIGHT 700; Carl Zeiss Meditec).

Binary RPE Damage Evaluation

As already mentioned, pulsed lasers with high CW power and variable pulse duration in the microsecond range are currently being investigated for SRT. Therefore, an in vivo dataset regarding RPE damage thresholds for laser pulses of 8, 12, 16, and 20 µs was generated by performing a probit analysis based on ICGA

images. For this purpose, all threshold pattern lesions of all rabbits were evaluated in a binary fashion via an area-based pass/fail detection criterion. Successful RPE damage was assumed if the treated hyperfluorescent area within the 223 × 223-µm^2 top-hat beam profile exceeded or fell below 50% of the lesion-size, thus receiving scores of 1 and 0, respectively. The ICGA post-processing and lesion-size evaluation was accomplished with Fiji in ImageJ (National Institutes of Health, Bethesda, MD).[38] The probit analysis was performed with Origin 2019b (OriginLab Corporation, Northampton, MA) utilizing the Levenberg Marquardt iteration algorithm to fit with a χ^2 tolerance value of 1×10^{-9} within up to 400 iteration steps. This analysis provided the median effective dose irradiation threshold (ED_{50}). An ED_{50} irradiation value means that 50% of treatments at this irradiation level depict observable RPE lesions. The corresponding ED_{15} and ED_{85} values were calculated to visualize the width of the fitted normal distribution in a logarithmic covariant basis.[39] In addition to ICGA imaging, OCT B-scans were acquired simultaneously over the threshold pattern in some animals to compare morphological changes with RPE lesion formation. However, the main focus was on large-scale RPE removal, which is why a comprehensive dataset is not available for the threshold pattern and only initial results are addressed in the discussion.

Results

Multimodal Imaging After Laser Therapy

Within 1 hour after laser irradiation, the treatment effects for the RPE damage threshold pattern and large-area laser microsurgery were investigated using IR, FA, ICGA, and SD-OCT. In IR imaging, the treated area is encircled by a hyporeflective border (Fig. 2a). The FA examination of the retina showed normal filling of large choroidal and retinal vessels in the early phase, suggesting that no coagulative damage within the choroid was induced (Fig. 2b). The laser-treated area, however, became clearly visible in the late phase (Fig. 2c), suggesting a compromised outer blood–retinal barrier. In the early phase of the ICGA, a normal perfusion in large choroidal vessels (Fig. 2d) can be recognized. In the mid phase, the treatment pattern started to become visible along with focal hyperfluorescence (Fig. 2e), which remained visible in the ICGA late phase, with the treatment pattern becoming clearly demarcated by ICG dye accumulation (Fig. 2f). The corresponding SD-OCT scan taken through the center of the irradiation pattern (green line in Fig. 2f) shows normal reflective bands throughout the treated area without any signs of outer retina damage (Fig. 2g).

Large-Area RPE Removal

A threshold pattern was used to define the target energy (Figs. 1a, 1b) for large-area RPE removal. The laser-induced effects visible in IR cSLO 3 minutes after the laser irradiation (Fig. 1d) were similar to the effects seen in the late phase ICGA images (Fig. 1b). Further confirmation of mild FA leakage and the absence of increased hyperreflectivity in the outer retinal bands within a laser-treated area led to the validation of IR cSLO imaging as a rather simple, non-invasive predictive biomarker for the laser settings. Typical laser energies using 8 µs single pulses for large-area RPE removal were 55 µJ (111 mJ/cm^2) (Fig. 3, Fig. 4) to 61 µJ (123 mJ/cm^2) (Fig. 2). These laser parameters were shown to result in large-area RPE removal without morphological retinal changes beyond the ellipsoid zone (EZ) (Figs. 2–4). Furthermore, we experimented with increasing areas of confluent laser spots ranging from 8.1 mm^2 (Fig. 4) to maximal 13.6 mm^2 (Fig. 2). To achieve control over the direction of the bRD formation, we also tested two different laser pattern designs, square and bottle. Both shapes could be achieved (compare Fig. 2 and Fig. 4).

RPE Cell Damage Thresholds After Single Pulse Irradiation

In total, 640 laser lesions were applied to the retina in 10 eyes of nine rabbits. Out of these, nine eyes with 576 treatment spots altogether were included in the evaluation. One eye was excluded because an evaluation was not possible due to insufficient ICGA image quality. This quantity of laser lesions applied has proven to be sufficient for probit analysis. The resulting radiant exposure thresholds values for RPE cell damage after single pulse laser irradiation are summarized in the Table.

bRD Formation After Laser Therapy

The laser irradiated regions were visible under the surgical microscope (Fig. 3d) and did not require demarcation by photocoagulation (see Supplementary Movie S1). Due to operator problems, intraoperative OCT could not be performed for the laser-irradiated area with the retina still attached. For the purpose of subretinal injection, the bottle shape proved more advantageous, as the bottle neck served as a

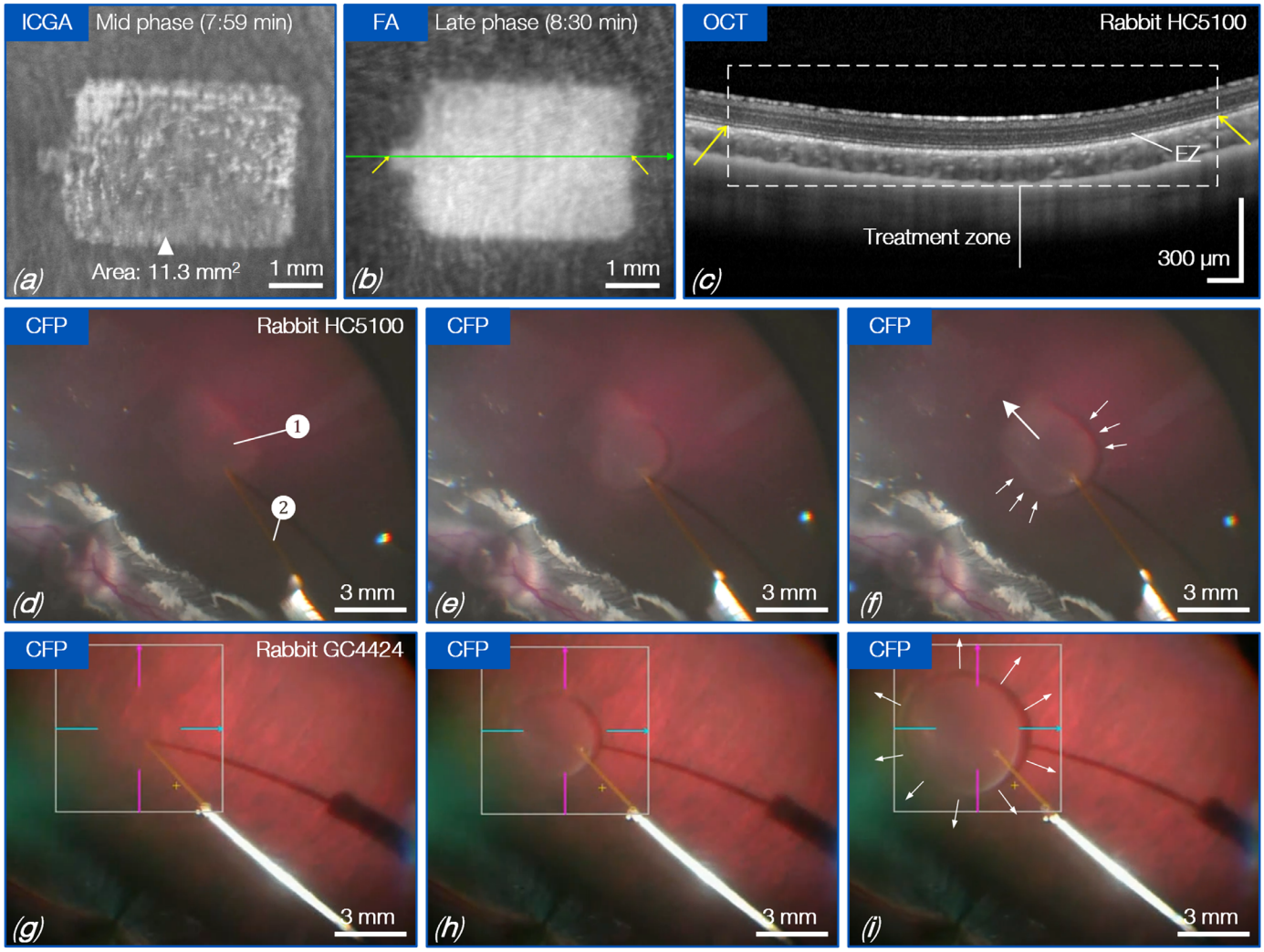

Figure 3. Macroscopic effects of laser-induced large-area RPE removal on the formation of a bRD. (a, b) For late phase ICGA and FA after treatment, the treatment pattern was clearly visible. The laser-irradiated area was 11.3 mm^2. Single laser pulses of 8 µs duration with a pulse energy of 55 µJ (111 mJ/cm^2) were applied. (c) The *green line* demarcates the cross-section in the corresponding SD-OCT B-scan displayed; *yellow arrows* encompass the treated zone. The B-scan through the irradiated RPE area showed no changes in morphology or backscatter. (d) Intraoperative CFP prior to bRD formation of the same rabbit. *Label 1* depicts the pretreated area, and *label 2* points at the tip of the subretinal cannula. (e, f) Following intraoperative CFP during bRD formation, the fluid followed the laser-irradiated area in a controlled manner, away from subretinal cannula 8. (g) Intraoperative CFP prior to bRD formation in an untreated rabbit eye. (h, i) In the following intraoperative CFP during bRD formation, a circular bleb formed uncontrollably around the subretinal cannula. The *white arrows* indicate the direction of bleb formation.

landing area for the subretinal cannula (Fig. 3a). Angiography and OCT performed prior to surgery confirmed the selective laser effect on the RPE without affecting choroidal perfusion (Figs. 3a, 3b) or adjacent retina (Fig. 3c). The slowly subretinal injected BSS followed the predefined laser path to gradually adopt a "half-cylindrical" bRD (Figs. 3d–3f), indicating lower resistance above the laser-irradiated RPE. When BSS was injected above the laser-treated area, bRD formation progressed smoothly without pauses (see Supplementary Movie S1). By contrast, in bRD controls raised over RPE not treated by SRT, the bleb expanded uncontrolled, in no preferred direction, while forming a round base shape (Figs. 3g–3i); here, micro pauses could be appreciated during the injection and more fluid volume was required to inject an area comparable to laser-treated blebs (see Supplementary Movie S2).

Intraoperative OCT of the bRD Formation

During subretinal injection over laser-irradiated areas, the intraoperative OCT documented a rather low bRD with shallow angles (Figs. 4c–4e; Supplementary Movie S3). By contrast, when imaging the bRD

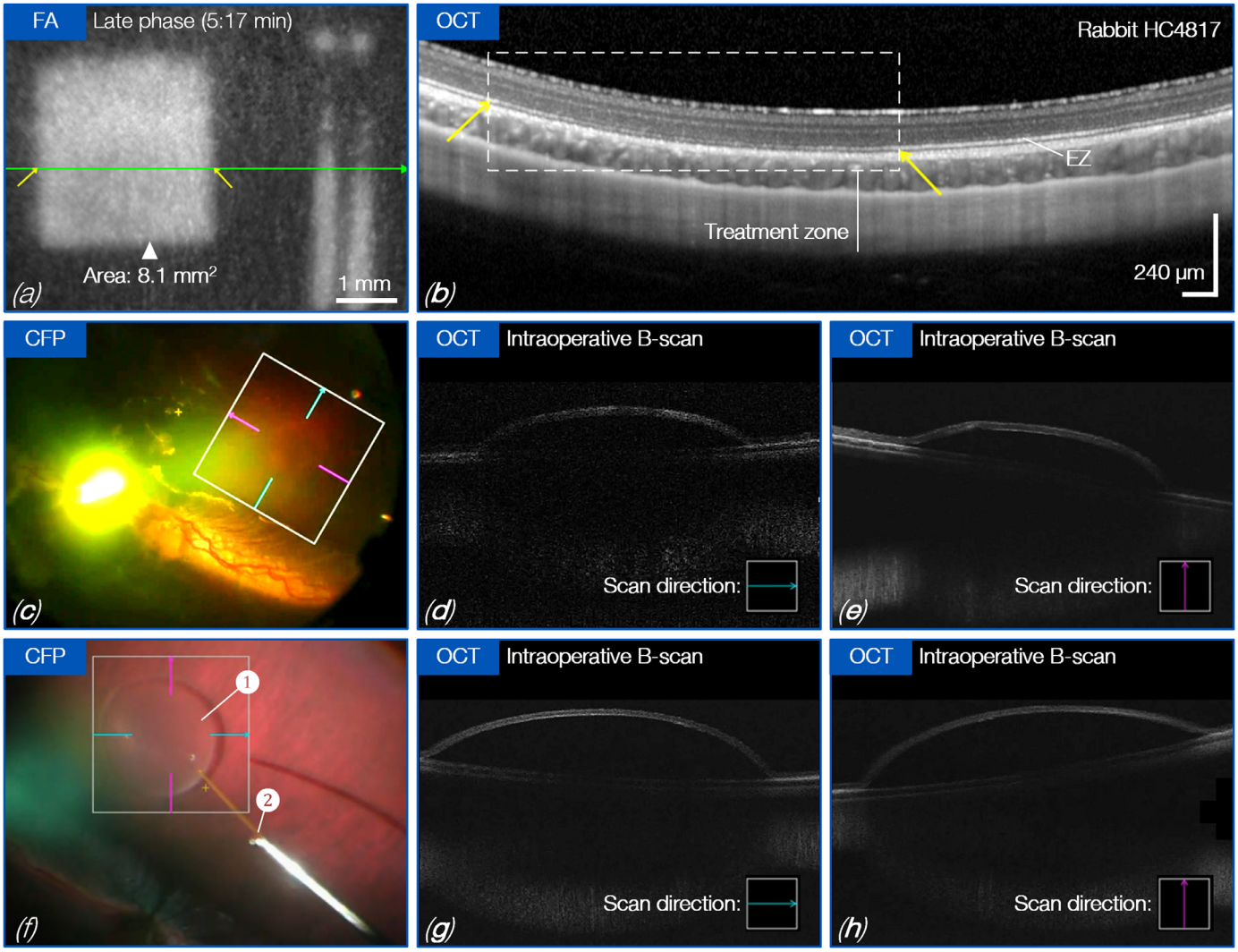

Figure 4. Microscopic effect of large-area RPE removal on the formation of a bRD. (a) for late phase FA after treatment, the treatment pattern is clearly visible. The laser irradiated area is 8.1 mm^2. Single laser pulses of 8 µs duration with a pulse energy of 55 µJ (111 mJ/cm^2) were applied. (b) The *green line* demarcates the displayed cross-section in the corresponding SD-OCT B-scan image. The *yellow arrows* are set at the border of the treated area. The B-scan through the irradiated RPE area showed no visible morphological changes or brightening of the outer retina. (c) Intraoperative CFP after bRD formation of the same rabbit. The *blue* and *pink lines* demarcate the displayed cross-section in the corresponding intraoperative OCT B-scan images. (d, e) The corresponding B-scans show a narrow bRD with a shallow angle. (f) Intraoperative CFP after bRD formation of an untreated rabbit eye. (g, h) The corresponding OCT showed a wide bRD with a steeper angle.

formation in the untreated control (Fig. 4f), the bRD appeared more convex, with steeper angles at the edges (Figs. 4g, 4h; Supplementary Movie S4).

Discussion

To achieve replacement of dysfunctional RPE with a cell therapeutic, several groups have investigated methods of RPE removal in animal experiments. Some surgical methods caused trauma to Bruch's membrane and/or choriocapillaris,[40] and other studies have reported damage to the outer retina.[15,41] We have recently described a method for RPE removal with an extendible prolene loop,[37] which generates a roughly 2 × 3-mm^2 RPE wound that will be repopulated with RPE and microglial multilayers, suggesting aberrant wound healing (Al-Nawaiseh S, Kroetz C, Rickmann A, et al., unpublished manuscript). Furthermore, the technique requires a rather large retinotomy to gain access to the subretinal space. Particularly for RPE suspension transplant approaches, both latter aspects may severely compromise proper subretinal graft integration.

Table. Angiographic Probit Analysis Providing the ED_{50} , ED_{15}, and ED_{85} Values for RPE Cell Damage for In Vivo Microsecond Single Pulse Laser Exposure

	Angiographic Probit Analysis					
	ED_{15}		ED_{50}		ED_{85}	
Exposure Time (µs)	µJ	mJ/cm^2	µJ	mJ/cm^2	µJ	mJ/cm^2
8	40	80	45	90	51	102
12	46	92	52	104	58	116
16	57	114	59	118	60	120
20	64	128	71	142	78	156

Note: Due to the area-based evaluation criterion for the binary lesion assessment, the intensity modulation factor was not included in the probit analysis.

Contrary to the RPE wound healing after surgical debridement, the use of SRT demonstrated local RPE debridement without negatively effecting the choroidal perfusion or the neurosensory retina.[17] Furthermore, several groups have independently demonstrated RPE repopulation by migration and proliferation after SRT, as well as preservation of photoreceptors.[25,42,43] Nevertheless, large-area SRT to solely remove the RPE remains a technical challenge. To the best of our knowledge, only the Palanker group has successfully attempted a similar approach for large-scale (2 × 2 mm) retinal tissue destruction by selective photocoagulation of RPE cells as well as photoreceptors with a scanning laser.[25] However, their goal was not to reduce choroidal retinal attachment but rather to create an animal model with local retinal degeneration. Furthermore, Sharma et al.[44] recently used a 532-nm micropulse laser to selectively treat an RPE region in preparation for 4 × 2-mm RPE patch delivery for the purposes of creating an RPE/photoreceptor injury model rescued by subsequent pluripotent RPE stem cell induction. Compared with the studies mentioned above, the pattern for large-area RPE removal within this study was applied in a pulse-by-pulse fashion rather than using a continuous scanning laser approach. However, the advantage of a scanning laser is the processing speed. Lorach et al.[25] worked with a scanning speed of 1.6 m/s (local retinal exposure, 60 µs) to treat a 2 × 2-mm retinal damage zone. Our largest pattern of 11.3 mm would therefore have been processed in approximately 40 ms (beam profile of 223 × 223 µm^2). The SPECTRALIS CENTAURUS system, which was built for the classical SRT protocol that clinically intends the application of single lesions, required several minutes. Technically, this time could easily be reduced to less than 1 minute, but achieving a similar time as the scanning approach would be difficult. However, by using a multispot pulse-by-pulse pattern, the advantage might be the possibility of applying eye tracking and local laser pulse energy dosing. Eye tracking could immediately correct unintentional eye movements during laser application and automatically correct overlaps respectively gaps within the pattern. In addition, the pulsed multispot pattern would allow final energy dosing of each individual lesion, an aspect that is extremely important for SRT and which is addressed later in this article.

The optical delamination process of the retina and choroid in this work was induced by microsecond laser pulses. It primarily affects RPE melanosomes that superheat, causing nearby intracellular fluid to produce microbubbles, which then form a pressure wave that destroys cellular membranes. According to this model, the SRT damage heavily involves the melanin-rich apical microvilli of the RPE that interface with photoreceptor outer segments. Due to elevated melanin levels nearby, the apical circumferential zonulae occludentes in this cytoskeletal structure are likewise prone to damage.[45] IR, FA, and ICGA imaging of exposure sites seems to support this model. In late phase FA, the exposed region is highlighted by mild hyperfluorescence, but the ICGA clearly delineates the altered RPE with hyperfluorescence in the late phase. Neither FA nor ICGA hints toward any choroidal vascular leakage and unstructured macroscopic hemorrhage, suggesting that the endothelium is not affected by the laser–tissue interaction. Meanwhile, late phase or mid phase ICGA (Fig. 2e) revealed an interesting behavior of cell patches, which seemingly experienced slightly lower heating during the laser exposure, potentially due to physiological fluctuations of absorbance or laser conditions. In particular, the cell patches at the periphery of the treated region, extending between the fenestrations to the center and caused by more efficient laser removal, hyperfluoresced with respect to untreated tissue, in obvious contrast to the heavily affected regions. Inside the treatment region, islands of normally appearing cells featured a similar fluorescence as the surrounding tissue. Assuming that the intact RPE in mid phase ICGA is typically dominated by the autofluorescence of the tissue,[46] rather than the dye, the relative brightening of cellular patches could be associated with selective dye uptake of active, still vital cells from the freely floating interstitial fluid or alternatively to ruptured tight junction complexes, as discussed above. The late phase ICGA (Fig. 2f) further accentuated these effects, such that hyperfluorescent regions kept their higher levels and the islands succumbed to similarly reduced fluorescence levels like the untreated regions.

When comparing ICGA and OCT (Figs. 5, 6), it appears that an appreciable outer retinal OCT hyperreflectivity was only associated with heterogenization of refractive indices from denaturation at significantly

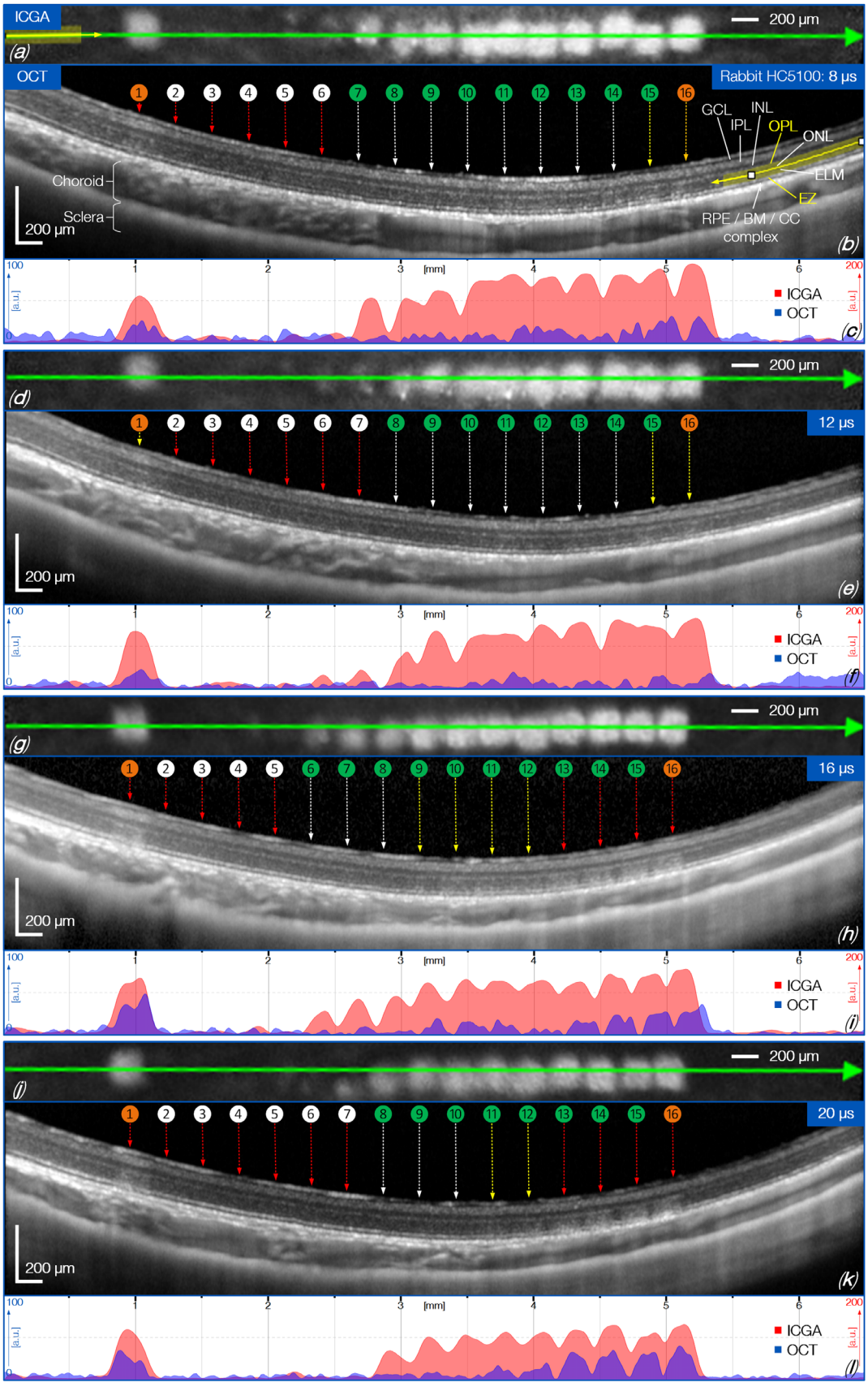

Figure 5. Threshold pattern applied with laser pulses 8, 12, 16, and 20 µs in duration and increasing treatment energy (from left to right) in rabbit HC5100. (a, d, g, j) Late phase ICGA images show the laser lesions. (b, e, h, k) *Green lines* demarcate the corresponding scan positions in

→

←
simultaneously captured SD-OCT B-scan images with numbered landmarks (1–16) for each lesion (*orange*, marker; *white*, no damage; *green*, damage). *Arrows* under the individual landmarks indicate whether the specified laser parameters are suitable or unsuitable for treatment of the respective lesion (*red*, unsuitable [potential over or under treatment]; *white*, suitable; *yellow*, possibly suitable). (c, f ,i, l) Grayscale overlap of ICGA lesions and the area between the EZ to the OPL of the corresponding OCT B-scans. For pulses of 16 and 20 µs duration, there was a correlation between ICGA lesions and morphological damage characteristics in OCT. For pulses of 8 and 12 µs, on the other hand, a larger treatment area (i.e., safety range) was apparent (lesions categorized as suitable). GCL, ganglion cell layer; IPL, inner plexiform layer; INL, inner nuclear layer; OPL, outer plexiform layer; ONL, outer nuclear layer; ELM, external limiting membrane; EZ, ellipsoid zone; RPE, retinal pigment epithelium; BM, Bruch's membrane; CC, choriocapillaris.

higher microsecond laser exposure levels. However, ICGA hyperfluorescence had already been triggered at much lower exposures. The two markers, therefore, do not necessarily correlate directly with levels of microscopic cellular damage. Upon examination of the response to different pulse durations, however, it can be observed that longer pulses led to more pronounced changes in retinal reflectance. Finally, the previously reported ability of IR cSLO to detect microbubble formation, which correlate well with ICGA and FA RPE indicators of permeability change thresholds, supports its use as a simple predictive biomarker imaging tool.

New compact pulsed laser sources with high CW power (up to 30 W) and variable pulse duration are currently being investigated for SRT, promising cellular specific removal at and close to the RPE.[23,24,33,47] To compare morphological changes with RPE lesion formation for pulses up to 20 µs duration, OCT B-scans were acquired simultaneously over the threshold pattern in addition to ICGA imaging in some animals. These initial results addressed the applicability of the different pulse durations. In some animals (e.g., rabbit HC5100) (Fig. 5), the safety interval for MBF-induced RPE damage without visible morphological change (white arrows, suitable) appeared to be slightly greater for 8 µs (8 pulses, $\Delta E = 38$ µJ) than for 20 µs (3 pulses, $\Delta E = 18$ µJ). Overlaying the ICGA lesions and the area between the EZ to the outer plexiform layer of the corresponding OCT B-scans highlights this difference in damage. However, despite ICGA hyperfluorescence, we did not detect any morphological tissue changes in SD-OCT B-scans at maximal pulse energy in various rabbits even for pulse durations of 12, 16, and 20 µs (e.g., rabbit JC0113) (Fig. 6). With respect to these initial results, however, it must be pointed out that it is not yet clear from these short-term studies whether or to what extent the photoreceptors were impaired at the time of exposure. Direct damage to individual photoreceptor segments, as well as other retinal layers and the choroid, cannot be definitively assessed with the imaging we performed; consequently, further longer term studies with histologic and immunohistochemical evaluation are necessary to detect and compare possible damage.

The phenomenon of varying retinal damage mentioned above is also likely to occur in the treatment of the human retina. The RPE damage threshold is known to vary both between patients and within retinal regions of individual patients because light absorption at the fundus varies based on the localized RPE melanosome density.[20] In addition to these RPE pigmentation-related variations, pathologic changes would also involve greater absorption, as well as topographic and morphological changes. To account for this inter- and intraindividual laser absorption, real-time laser dosimetry (i.e., absorption-corrected radiation exposure) would be essential for the clinical application of large-area RPE removal. Therefore, to conserve photoreceptor integrity, SRT irradiation must be kept just above the MBF threshold to avoid insufficient or excessive exposure effects. Currently, several approaches for real-time laser dosimetry are under development. Methods measuring the increased reflectance at the bubble surface via backscattered light or capturing the ultrasonic emission of vaporization to detect the appearance of MBF have been successfully tested.[48,49] Recently, we succeeded to reliably observe early stages of MBF formation with SD-OCT, thus enabling precise control of the damage level.[24] Regarding large-area RPE removal, further research is necessary to reveal particular situations for which laser applications can be adapted or are hindered by optical challenges, such as intransparency of the ocular medium or topological changes.

Subretinal injection to surgically induce a retinal detachment in rabbits results in well-documented trauma to the RPE and neural retina.[50,51] Although most of this undesirable effect is likely due to fluid turbulence in the subretinal space, tangential retinal stretching is also considered to be a contributor. Tan et al.[52] studied submacular BSS injection in nonhuman primates with intraoperative OCT. The most common complications were full-thickness foveal tears and/or cystoid foveal changes, phenomena that have also been seen in human gene therapy trials involving

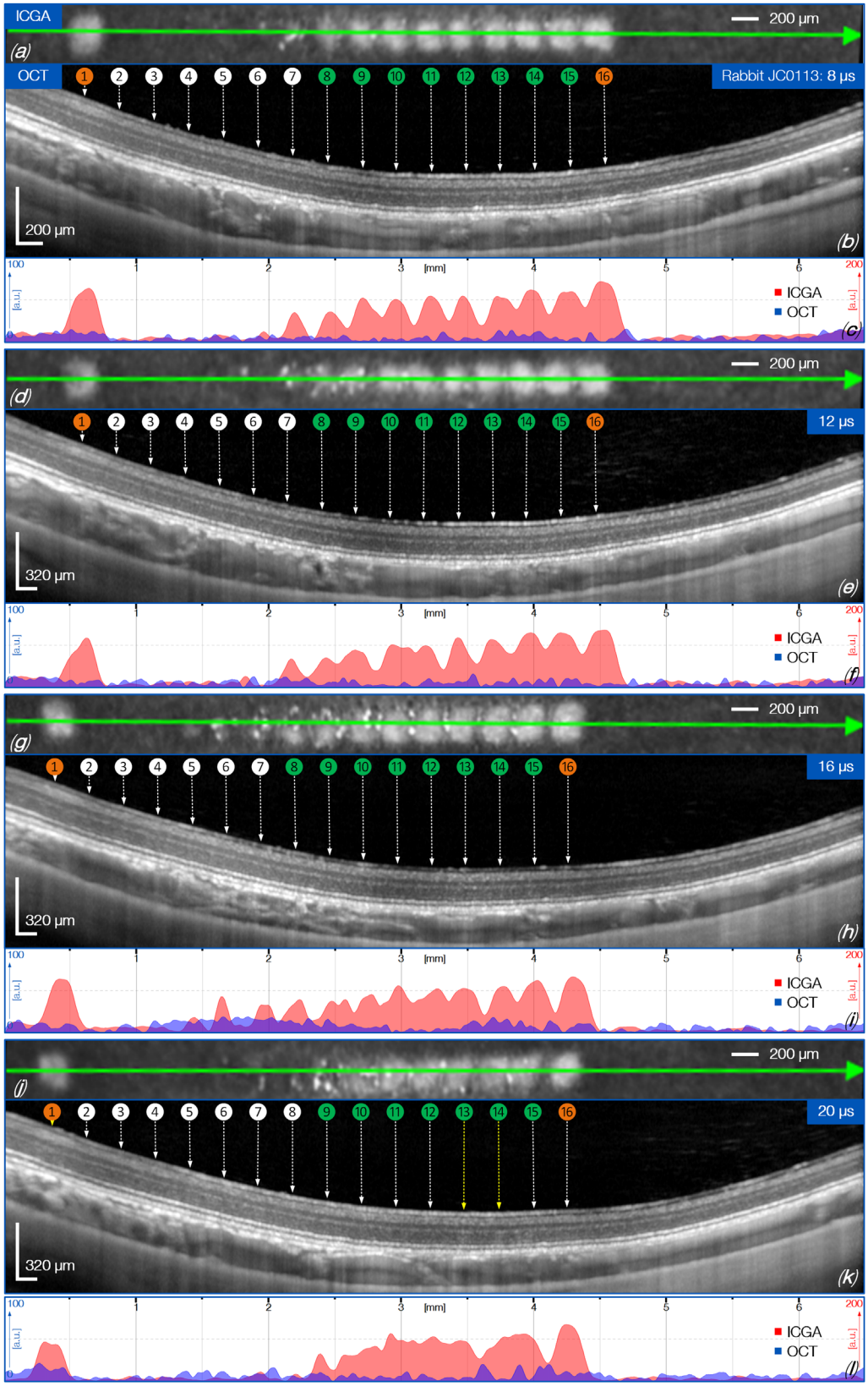

Figure 6. Threshold pattern applied with laser pulses of 8, 12, 16, and 20 µs and increasing treatment energy (from left to right) in rabbit JC0113 (evaluation similar to that of Fig. 5). There was no correlation for any pulse duration between ICGA lesions and morphological damage characteristics in OCT. For all pulse durations ranging from 2 to 20 µs, a larger treatment area (i.e., safety range) is shown compared with rabbit HC5100 (Fig. 5). For all lesions, no obvious morphological retinal changes beyond the EZ were present.

subretinal injection.[53,54] Modulating retinal adhesion has been shown to facilitate retinal detachment.[55] The use of SRT delamination appeared to significantly lower retinal adhesion, thereby resulting in a well-controlled bRD with presumably less tangential retinal stretching. In a clinical trial setting for RPE cell therapy such a tool would be a key enabler, as it standardizes access to the subretinal space. Combined with advanced intraoperative visualization, such as the surgical microscope-integrated OCT shown here, and robotics for precise subretinal injection could, over the long term, aid the adoption of RPE cell therapy in early disease stages.

One of the limitations of our study is that we manually injected BSS to form the bRD instead of using an automated infusion system, making it difficult to standardize the injection speed. We tried to overcome this problem by predefining the injected volume and having the same person (BVS) perform the injections (BVS). Furthermore, manual injection may cause more iatrogenic traumatic RPE damage than automated injection, and, if the transplantation is undertaken under the setting of choroidal neovascularization, the iatrogenic damage on the RPE is further minimized. This may exaggerate the effect of the laser on RPE damage. These limitations will be taken into consideration in future studies, when studying the long-term effects of laser treatment.

Acknowledgments

The authors thank the valuable support and the inspiring discussions with our colleagues Ralf Kessler, Stefan Schmidt, Michael Reutter, Joerg Fischer, Tilman Otto, and Kfir Azoulay from Heidelberg Engineering; Eric Odenheimer from Meridian AG; and Mustafa Arash from Carl Zeiss Meditec.

Supported by grants from the Swiss National Science Foundation (325230-141189 and 323523-163306) and from the Swiss Innovation Agency (KTI 25030.1 PFLS-LS: ReSight Consortium BMBF 01EK1613A to BVS; DFG STA 1135/2-1 to BVS).

Disclosure: **C. Burri**, Heidelberg Engineering (F), Meridian AG (F); **S. Al-Nawaiseh**, None; **P. Wakili**: None; **S. Salzmann**, None; **C. Krötz**, None; **B. Považay**, None; **C. Meier**, None; **M. Frenz**, None; **P. Szurman**, None; **A. Schulz**, None; **B. Stanzel**, Geuder (F, C, P), Carl Zeiss Meditec (F), MedOne Surgical (F), Vitreq (F)

* CB and SAN contributed equally to this work.

References

1. Bhagat N, Zarbin M. Recent innovations in medical and surgical retina. *Asia Pac J Ophthalmol (Phila)*. 2015;4:171–179.
2. Wong WL, Su X, Li X, et al. Global prevalence of age-related macular degeneration and disease burden projection for 2020 and 2040: a systematic review and meta-analysis. *Lancet Glob Health*. 2014;2:e106–116.
3. da Cruz L, Chen FK, Ahmado A, Greenwood J, Coffey P. RPE transplantation and its role in retinal disease. *Prog Retin Eye Res*. 2007;26:598–635.
4. van Zeeburg EJ, Maaijwee KJ, Missotten TO, Heimann H, van Meurs JC. A free retinal pigment epithelium-choroid graft in patients with exudative age-related macular degeneration: results up to 7 years. *Am J Ophthalmol*. 2012;153:120–127.e2.
5. Binder S, Stanzel BV, Krebs I, Glittenberg C. Transplantation of the RPE in AMD. *Prog Retin Eye Res*. 2007;26:516–554.
6. da Cruz L, Fynes K, Georgiadis O, et al. Phase 1 clinical study of an embryonic stem cell-derived retinal pigment epithelium patch in age-related macular degeneration. *Nat Biotechnol*. 2018;36:328–337.
7. Mandai M, Watanabe A, Kurimoto Y, et al. Autologous induced stem-cell-derived retinal cells for macular degeneration. *N Engl J Med*. 2017;376:1038–1046.
8. Kashani AH, Lebkowski JS, Rahhal FM, et al. A bioengineered retinal pigment epithelial monolayer for advanced, dry age-related macular degeneration. *Sci Transl Med*. 2018;10:eaao4097.
9. Schwartz SD, Regillo CD, Lam BL, et al. Human embryonic stem cell-derived retinal pigment epithelium in patients with age-related macular degeneration and Stargardt's macular dystrophy: follow-up of two open-label phase 1/2 studies. *Lancet*. 2015;385:509–516.
10. Sugita S, Mandai M, Hirami Y, et al. HLA-matched allogeneic iPS cells-derived RPE transplantation for macular degeneration. *J Clin Med*. 2020;9:2217.
11. Lopez PF, Yan Q, Kohen L, et al. Retinal pigment epithelial wound healing in vivo. *Arch Ophthalmol*. 1995;113:1437–1446.
12. Leonard DS, Zhang XG, Panozzo G, Sugino IK, Zarbin MA. Clinicopathologic correlation of localized retinal pigment epithelium debridement. *Invest Ophthalmol Vis Sci*. 1997;38:1094–1109.
13. Carido M, Zhu Y, Postel K, et al. Characterization of a mouse model with complete RPE loss and its

use for RPE cell transplantation. *Invest Ophthalmol Vis Sci*. 2014;55:5431–5444.
14. Petrus-Reurer S, Bartuma H, Aronsson M, et al. Integration of subretinal suspension transplants of human embryonic stem cell-derived retinal pigment epithelial cells in a large-eyed model of geographic atrophy. *Invest Ophthalmol Vis Sci*. 2017;58:1314–1322.
15. Del Priore LV, Hornbeck R, Kaplan HJ, et al. Debridement of the pig retinal pigment epithelium in vivo. *Arch Ophthalmol*. 1995;113:939–944.
16. Roider J, Hillenkamp F, Flotte T, Birngruber R. Microphotocoagulation: selective effects of repetitive short laser pulses. *Proc Natl Acad Sci USA*. 1993;90:8643–8647.
17. Brinkmann R, Roider J, Birngruber R. Selective retina therapy (SRT): a review on methods, techniques, preclinical and first clinical results. *Bull Soc Belge Ophtalmol*. 2006;302:51–69.
18. Roider J, Michaud NA, Flotte TJ, Birngruber R. Response of the retinal pigment epithelium to selective photocoagulation. *Arch Ophthalmol*. 1992;110:1786–1792.
19. Richert E, Koinzer S, Tode J, et al. Release of different cell mediators during retinal pigment epithelium regeneration following selective retina therapy. *Invest Ophthalmol Vis Sci*. 2018;59:1323–1331.
20. Gabel V-P, Birngruber R, Hillenkamp F. Visible and near infrared light absorption in pigment epithelium and choroid. In: Shimuzu K, Osterhuis JA, eds. *XXIll Concilium Ophthalmology Kyoto*. Amsterdam: Exerpta Medica; 1978:658–662.
21. Neumann J, Brinkmann R. Boiling nucleation on melanosomes and microbeads transiently heated by nanosecond and microsecond laser pulses. *J Biomed Opt*. 2005;10:024001.
22. Neumann J, Brinkmann R. Cell disintegration by laser-induced transient microbubbles and its simultaneous monitoring by interferometry. *J Biomed Opt*. 2006;11:041112.
23. Seifert E, Sonntag SR, Kleingarn P, et al. Investigations on retinal pigment epithelial damage at laser irradiation in the lower microsecond time regime. *Invest Ophthalmol Vis Sci*. 2021;62:32.
24. Burri C, Hutfliz A, Grimm LS, et al. Dynamic OCT signal loss for determining PRE radiant exposure damage thresholds in microsecond laser microsurgery. *Appl Sci*. 2021;11:5535.
25. Lorach H, Kung J, Beier C, et al. Development of animal models of local retinal degeneration. *Invest Ophthalmol Vis Sci*. 2015;56:4644–4652.
26. Alexander P, Thomson HA, Luff AJ, Lotery AJ. Retinal pigment epithelium transplantation: concepts, challenges, and future prospects. *Eye (Lond)*. 2015;29:992–1002.
27. Famiglietti EV, Sharpe SJ. Regional topography of rod and immunocytochemically characterized "blue" and "green" cone photoreceptors in rabbit retina. *Vis Neurosci*. 1995;12:1151–1175.
28. Rockhill RL, Daly FJ, MacNeil MA, Brown SP, Masland RH. The diversity of ganglion cells in a mammalian retina. *J Neurosci*. 2002;22:3831–3843.
29. Vaney DI, Gynther IC, Young HM. Rod-signal interneurons in the rabbit retina: 2. AII amacrine cells. *J Comp Neurol*. 1991;310:154–169.
30. Young HM, Vaney DI. Rod-signal interneurons in the rabbit retina: 1. Rod bipolar cells. *J Comp Neurol*. 1991;310:139–153.
31. Juliusson B, Bergstrom A, Rohlich P, Ehinger B, van Veen T, Szel A. Complementary cone fields of the rabbit retina. *Invest Ophthalmol Vis Sci*. 1994;35:811–818.
32. Sahl SJ, Hell SW, Bille JF, eds. *High Resolution Imaging in Microscopy and Ophthalmology: New Frontiers in Biomedical Optics*. Cham: Springer; 2019.
33. Hutfilz A, Burri C, Meier C, Brinkmann R. Ex vivo investigation of different µs laser pulse durations for selective retina therapy. In: Lilge LD, Philipp CM, eds. *Medical Laser Applications and Laser–Tissue Interactions IX*. Bellingham, WA: SPIE; 2019.
34. Framme C, Schuele G, Roider J, Kracht D, Birngruber R, Brinkmann R. Threshold determinations for selective retinal pigment epithelium damage with repetitive pulsed microsecond laser systems in rabbits. *Ophthalmic Surg Lasers*. 2002;33:400–409.
35. Roegener J, Brinkmann R, Lin CP. Pump-probe detection of laser-induced microbubble formation in retinal pigment epithelium cells. *J Biomed Opt*. 2004;9:367–371.
36. Lee H, Alt C, Pitsillides CM, Lin CP. Optical detection of intracellular cavitation during selective laser targeting of the retinal pigment epithelium: dependence of cell death mechanism on pulse duration. *J Biomed Opt*. 2007;12:064034.
37. Al-Nawaiseh S, Thieltges F, Liu Z, et al. A step by step protocol for subretinal surgery in rabbits. *J Vis Exp*. 2016;115:53927.
38. Schindelin J, Arganda-Carreras I, Frise E, et al. Fiji: an open-source platform for biological-image analysis. *Nat Methods*. 2012;9:676–682.
39. Sliney DH, Mellerio J, Gabel VP, Schulmeister K. What is the meaning of threshold in laser injury experiments? Implications for human exposure limits. *Health Phys*. 2002;82:335–347.

40. Ivert L, Kong J, Gouras P. Changes in the choroidal circulation of rabbit following RPE removal. *Graefes Arch Clin Exp Ophthalmol*. 2003;241:656–666.
41. Valentino TL, Kaplan HJ, Del Priore LV, Fang SR, Berger A, Silverman MS. Retinal pigment epithelial repopulation in monkeys after submacular surgery. *Arch Ophthalmol*. 1995;113:932–938.
42. Jeon SH, Kim M, Roh YJ. Retinal pigment epithelial responses based on the irradiation density of selective retina therapy. *Graefes Arch Clin Exp Ophthalmol*. 2021;259:101–111.
43. Kang S, Lorach H, Bhuckory MB, Quan Y, Dalal R, Palanker D. Retinal laser therapy preserves photoreceptors in a rodent model of MERTK-related retinitis pigmentosa. *Transl Vis Sci Technol*. 2019;8:19.
44. Sharma R, Khristov V, Rising A, et al. Clinical-grade stem cell-derived retinal pigment epithelium patch rescues retinal degeneration in rodents and pigs. *Sci Transl Med*. 2019;11:eaat5580.
45. Lakkaraju A, Umapathy A, Tan LX, et al. The cell biology of the retinal pigment epithelium [published online ahead of print February 24, 2020]. *Prog Retin Eye Res*. 2020.
46. Chang AA, Morse LS, Handa JT, et al. Histologic localization of indocyanine green dye in aging primate and human ocular tissues with clinical angiographic correlation. *Ophthalmology*. 1998;105:1060–1068.
47. Burri C, Hutfilz A, Grimm L, et al. Optical coherence tomography controlled selective retina therapy with a novel microsecond laser. In: Brown JQ, van Leeuwen TG, eds. Clinical and Preclinical Optical Diagnostics II. Bellingham, WA: SPIE; 2019.
48. Schuele G, Elsner H, Framme C, Roider J, Birngruber R, Brinkmann R. Optoacoustic real-time dosimetry for selective retina treatment. *J Biomed Opt*. 2005;10:064022.
49. Seifert E, Roh Y-J, Fritz A, et al. Automatic irradiation control by an optical feedback technique for selective retina treatment (SRT) in a rabbit model. In: Lilge L, Sroka R, eds. Medical Laser Applications and Laser–Tissue Interactions VI. Bellingham, WA: SPIE; 2013:880303.
50. Szurman P, Roters S, Grisanti S, et al. Ultrastructural changes after artificial retinal detachment with modified retinal adhesion. *Invest Ophthalmol Vis Sci*. 2006;47:4983–4989.
51. Bartuma H, Petrus-Reurer S, Aronsson M, Westman S, Andre H, Kvanta A. In vivo imaging of subretinal bleb-induced outer retinal degeneration in the rabbit. *Invest Ophthalmol Vis Sci*. 2015;56:2423–2430.
52. Tan GSW, Liu Z, Ilmarinen T, et al. Hints for gentle submacular injection in non-human primates based on intraoperative OCT guidance. *Transl Vis Sci Technol*. 2021;10:10.
53. Xue K, Groppe M, Salvetti AP, MacLaren RE. Technique of retinal gene therapy: delivery of viral vector into the subretinal space. *Eye (Lond)*. 2017;31:1308–1316.
54. Maguire AM, Simonelli F, Pierce EA, et al. Safety and efficacy of gene transfer for Leber's congenital amaurosis. *N Engl J Med*. 2008;358:2240–2248.
55. Marmor MF. Mechanisms of normal retinal adhesion. In: Ryan SJ, Wilkinson P, eds. *Ryan's Retina*, 4th ed. St. Louis, MO: Mosby; 2005:1891–1908.

Supplementary Material

Supplementary Movie S1. Intraoperative video showing the formation of a bleb retinal detachment after selective microsecond laser-based large-area RPE removal.

Supplementary Movie S2. Intraoperative video showing the formation of a bleb retinal detachment over untreated healthy RPE.

Supplementary Movie S3. Intraoperative video showing the formation of a bleb retinal detachment after selective microsecond laser-based large-area RPE removal with live feedback using an intraoperative OCT.

Supplementary Movie S4. Intraoperative video showing the formation of a bleb retinal detachment over untreated healthy RPE with live feedback using an intraoperative OCT.